Isolated cumulus congestus based on SCMS campaign: comparison between Eulerian bin and Lagrangian particle-based microphysics

Case coordinators:

Dr. Shin-ichiro Shima (s_shima@sim.u-hyogo.ac.jp)
Dr. Wojciech W. Grabowski (grabow@ucar.edu)

Timeline

Dec 2019:	Announcement
30 Jan 2020:	Confirmation of participation
Around 15 May 2020:	1st communication with participants
Around 15 Jun 2020:	2nd communication with participants
27-31 Jul 2020:	ICMW workshop

Overview

Width of the droplet size distribution affects radiative properties of warm (ice-free) clouds and likely impacts formation of precipitation through collision/coalescence. One can argue that warm rain formation in bin microphysics models is affected by artificial spectral broadening in bin schemes (Morrison et al. 2018, Grabowski et al. 2019). Lagrangian particle-based schemes, on the other hand, are free from those problems, but may impact simulated cloud properties because of limited (and typically relatively small) number of super-droplets that can be used. This case aims at comparing cloud droplet distributions simulated by applying either spectral bin microphysics or Lagrangian particle-based microphysics. The modeling case is based on previous simulations of a case from the Small Cumulus Microphysics Study (SCMS) field campaign that took place in 1995 in Florida (USA) as described in Lasher-Trapp et al. (2005, L05 hereinafter). 2D and 3D simulations are considered. Although computationally expensive, 3D simulations allow realistic simulations of cloud dynamics (e.g., turbulence) and cloud microphysics. In comparison to 3D, 2D simulations allow relatively inexpensive tests of the impact of model resolution, number of bins used in bin simulations, and number of super-droplets applied in Lagrangian simulations on model results. Our suggestion is to start with 2D simulations and develop a sensible setup for 3D simulations. Below, we briefly discuss observations of natural clouds in SCMS field project and subsequently describe the modeling setup.

Microphysical characteristics of cumuli observed in SCMS depend on the origin of the air mass in which convection developed (i.e., maritime versus continental). Brenguier et al. (2011) reports statistics of droplet population observed by Fast-FSSP in SCMS. The table below reproduced from Brenguier et al. (2011) shows the statistics for SCMS.

Table 4. Summary of the data set with for each flight the mean and standard deviation σ of CDNC $\langle N\rangle$ and k values $\langle k\rangle$, the k^* value, the ratio of k^* to $\langle k\rangle$, the N_{act} parameter, the ratio N/N_{act}, the mean LWC adiabatic fraction $\langle q_{\mathrm{c}}/q_{\mathrm{cad}}\rangle$ and the cumulated length of cloudy samples L_{c}. The last line for each data set shows the mean values, except for the last column that shows the total length of cloudy samples.

Date	$\langle N\rangle \pm\sigma$ (cm^{-3})	$\langle k\rangle \pm\sigma$	k^*	$k^*/\langle k\rangle$	N_{act} (cm^{-3})	N/N_{act}	$\langle q_{\mathrm{c}}/q_{\mathrm{cad}}\rangle$	L_{c} (km)
SCMS (1995)								
22/07	294 ± 243	0.825 ± 0.060	0.692	0.839	926	0.318	0.213	23.8
24/07	329 ± 235	0.830 ± 0.069	0.707	0.852	759	0.434	0.246	47.9
04/08	120 ± 62	0.811 ± 0.085	0.788	0.972	224	0.536	0.324	70.6
05/08	121 ± 60	0.802 ± 0.074	0.801	0.999	218	0.555	0.321	49.7
06/08	152 ± 72	0.867 ± 0.071	0.759	0.875	274	0.555	0.263	74.8
07/08	225 ± 175	0.819 ± 0.100	0.703	0.858	683	0.329	0.259	56.0
08/08	325 ± 255	0.817 ± 0.052	0.792	0.969	940	0.346	0.264	37.8
09/08	186 ± 123	0.858 ± 0.056	0.805	0.938	447	0.416	0.447	26.7
10/08	129 ± 82	0.843 ± 0.077	0.744	0.883	250	0.516	0.344	46.5
11/08	194 ± 118	0.823 ± 0.079	0.739	0.898	424	0.458	0.288	36.5
12/08	312 ± 185	0.840 ± 0.049	0.754	0.898	670	0.466	0.400	19.8
mean	**217**	**0.831**	**0.753**	**0.907**	**529**	**0.448**	**0.306**	**490.1**

Case specification (3D)

The figure below shows the initial sounding.

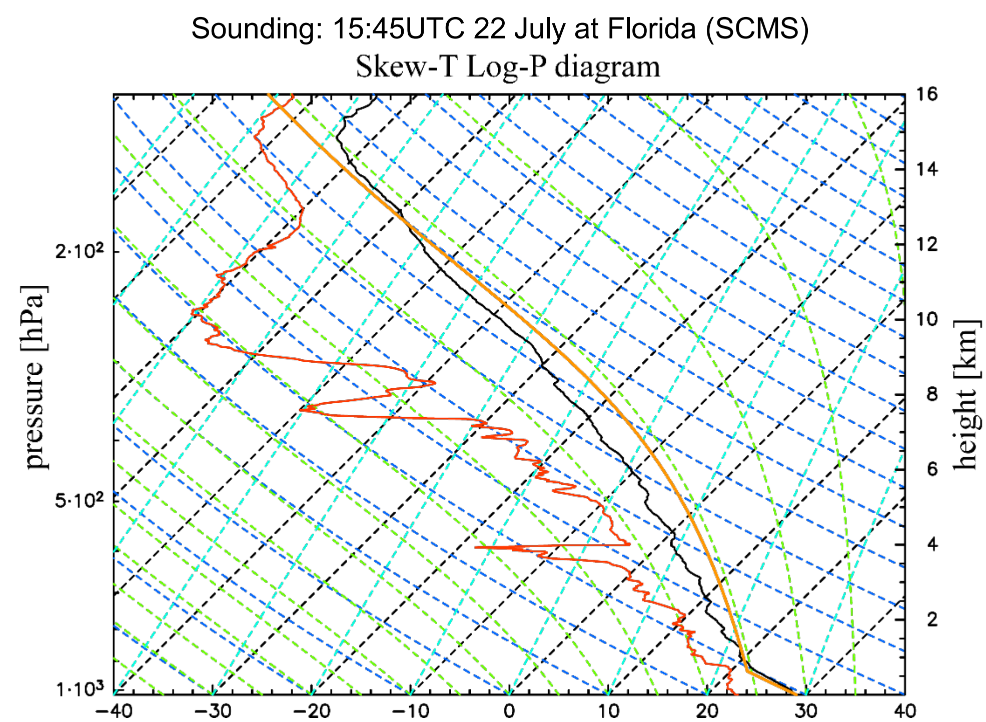

The sounding data (provided by courtesy of Dr. Lasher-Trapp) is available from the following link: https://drive.google.com/file/d/1629xTs7gaBH42ZlGaJXPqm7RVyLEiX3v. The variables on the first line represent surface pressure [hPa], surface potential temperature [K], and surface specific humidity [g/kg], respectively. The variables from the second line represent the state of atmosphere at each level; the columns represent height [m], potential temperature [K], specific humidity [g/kg], and *x*- and *y*-components of wind velocity [m/s], respectively. The data feature a fairly detailed representation of the temperature and moisture stratification, with about 400 levels between the surface and 100 hPa. Although one may consider applying some smoothing to the sounding, we decided not to do this. Note that having very detailed sounding may have an impact on the comparison of simulations applying different vertical grid lengths. This is because high resolution includes more structure of the initial sounding that is not resolved with a lower resolution. This aspect is beyond the scope of the initial simulations and may be pursued in the future. Also, as in L05 we exclude collision/coalescence in initial set of simulations, but encourage participants to consider rain development in follow-up studies.

CCN representation should be taken as discussed in section 2b(ii) in L05, that is, applying the Twomey formula: $N = 1114\ S^{0.77}$, where N in the concentration of activated droplets (in cm^3) and S is the supersaturation in %. The maximum concentration N is limited to 1150 cm^{-3}. For models requiring more information about CCN size, chemical composition, etc., we suggest to use an aerosol distribution which is made by increasing the number concentration 11 times from that given in van Zanten et al. (2011) for RICO intercomparison case. The aerosol particles are composed of ammonium bisulfate, and the number-size distribution is given by a bimodal log-normal distribution: The particle number concentrations of the two modes are N_1 = 11x90 cm^{-3} and N_2 = 11x15 cm^{-3}, respectively; the geometric mean radii are r_1 = 0.03 μm and r_2 = 0.14 μm, with geometric standard deviations of σ_1 = 1.28 and σ_2 = 1.75, respectively. As the figure below shows, the CCN activation characteristics are similar, but not the same. The red and black dashed lines represent the Twomey formula and 11 times increased van Zanten et al.'s (2011) distribution, respectively. To plot the black dashed line, we assumed that the cloud base temperature is 20 ℃.

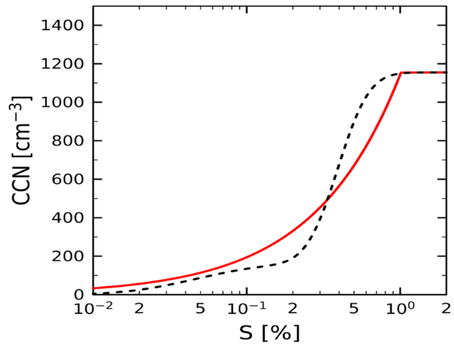

Computational domain should be 10 km x 10 km in the horizontal and 8 km in the vertical (10 km top would be better, if possible, especially when applying Rayleigh dumping). The grid length should be 50 m as in L05. The domain should be periodic in the horizontal. The upper boundary is a free-slip rigid-lid. At the lower boundary we impose surface fluxes as described below.

L05 developed a method to force a cloud developing from a turbulent convective boundary layer as in nature. We follow the same approach. For the initial one hour of the simulation, horizontally-uniform surface sensible and latent heat fluxes are applied. The surface sensible and latent heat fluxes should be taken as

$$\overline{q_v'w'} = 0.4 \times 10^{-4}\ \mathrm{kg\ kg^{-1} m\ s^{-1}},$$
$$\overline{\theta'w'} = 0.1\ \mathrm{K\ m\ s^{-1}}.$$

To initiate convection, specific humidity q_v and potential temperature θ are perturbed initially by adding random noise to the lowest 1 km layer with amplitudes 2.5 x 10^{-5} kg kg^{-1} and 0.01 K, respectively. This leads to the development of boundary-layer eddies that modulate formation of a cloud. For the second hour, the uniform surface fluxes are replaced by surface fluxes with a Gaussian distribution centered in the middle of the domain. The maximum of the Gaussian flux is supposed to be three times larger than the uniform flux (i.e., as 0.3 K m s^{-1} and 1.2 x 10^{-4} kg kg^{-1} m s^{-1}) and the half-width of the distribution should be taken as 1.7 km.

$$\overline{q_v'w'} = 1.2 \times 10^{-4}\ \mathrm{kg\ kg^{-1} m\ s^{-1}}\ \exp\left[-\frac{(x-5\ \mathrm{km})^2 + (y-5\ \mathrm{km})^2}{(1.7\ \mathrm{km})^2}\right],$$
$$\overline{\theta'w'} = 0.3\ \mathrm{K\ m\ s^{-1}} \exp\left[-\frac{(x-5\ \mathrm{km})^2 + (y-5\ \mathrm{km})^2}{(1.7\ \mathrm{km})^2}\right].$$

The momentum flux at the surface is given by a constant friction velocity:

$$\overline{u'w'} = \frac{(0.28\ \mathrm{m\ s^{-1}})^2}{\max(|\boldsymbol{U_1}|,\ 10^{-4}\mathrm{m\ s^{-1}})} u_1,$$
$$\overline{v'w'} = \frac{(0.28\ \mathrm{m\ s^{-1}})^2}{\max(|\boldsymbol{U_1}|,\ 10^{-4}\mathrm{m\ s^{-1}})} v_1,$$

where $\boldsymbol{U}_1=(u_1,v_1)$ is the horizontal velocity vector at the first model layer above the surface.

Rayleigh dumping can be included in the uppermost 1 km of the domain, but it is not required. SGS turbulence scheme is recommended, but also not required. Only droplet activation and condensational growth need to be included in the initial simulations. Droplet sedimentation can be included although its impact is likely negligible considering the vertical grid length. The number of bins in the Eulerian bin scheme and the number of super-droplets in Lagrangian particle-based microphysics should be selected by the user to ensure numerical convergence. For single moment bin schemes, we recommend applying 30-50 bins with a bin width of a few tenths of 1 micron. Stretched bin layout can also be considered to minimize the impact of numerical spreading. For Lagrangian particle-based microphysics, we recommend applying at least 30 super-droplets per grid box. Finally, we suggest to use a small ensemble of simulations to eliminate the impact of different flow realizations, or – if possible – application of the piggybacking methodology (Grabowski 2019).

Case specification (2D)

The 2D simulations are supposed to serve as an efficient testbed for various parameters. The 2D domain is slightly larger, 12 km in the horizontal, and the same (8 or 10 km) in the vertical, with the same boundary conditions. The grid length should be taken as 50 m in both directions. Simulations can be run longer, say, for 3 hours. The forcing is similar as in the 3D case.

Our preliminary tests suggest that 2D simulations are more sensitive to latent/sensible heat flux than 3D simulations; if the flux is too strong, the cloud can reach the top of the domain because the equilibrium height of the initial sounding is about 13 km. If it does happen, please consider decreasing the surface flux for the 2D case.

Sensitivity tests (3D and 2D)

For assessing the sensitivity, we recommend considering:

- modifying the spatial resolution (from 50 m down to as high as possible);

- modifying the CCN number concentration (however, reducing the concentration too far is unrealistic as pristine clouds as deep as in the L05 simulation would likely precipitate heavily);
- modifying the structure and number of bins in the droplet radius/mass grid;
- modifying the number of super-droplets (say, to a few hundred per grid box);
- including collision/coalescence

Recommended output (3D)

We do not specify recommended output, but participants are recommended to provide the following plots and data. See also Section “Definitions” for more details about the variables, and Section “Example of results”.

x-*z* cross section in the middle of the forcing area
- mass concentration of cloud droplets q_c (and rain drops q_r for the case with collision/coalescence)
- number concentration of droplets n
- effective radius r_e
- standard deviation of the droplet size distribution σ
- ratio of mean volume radius to effective radius cubed k (see the table from Brenguier et al. above)
- liquid water content LWC
- adiabatic fraction AF (the ratio of the LWC and the adiabatic LWC, ALWC, see below).

Vertical profile (2D histogram, median of cloudy grid cells at each height, 5th and 95th percentiles, etc.) of
- number concentration of droplets n
- effective radius r_e
- standard deviation σ
- ratio of mean volume radius to effective radius cubed k
- liquid water content LWC
- adiabatic fraction AF

Time series of
- cloud top height CTH
- total number of droplets N^{tot}
- total liquid water mass LWM^{tot}, cloud water mass CWM^{tot}, and rain water mass RWM^{tot} (the first and the last for the case with collision/coalescence)
- accumulated precipitation amount at the surface.

Computational cost

- number of CPU cores and wall clock time

Additionally, we are also thinking of comparing the droplet size distribution (DSD) though it would be not easy due to the unsteadiness of the cloud evolution and differences in the flow realization. Therefore, participants are encouraged to plot the DSDs applying some criteria. Averaging DSDs globally is one possibility, although we expect this will be not very informative. Selecting several representative times and locations is another idea. For instance, one can compare DSDs by selecting a specific height and then grouping DSDs based on the AF. This can be done for various time levels.

Recommended output (2D)

Same as 3D but extensive variables should be replaced by per y-axis length quantities.

Definitions

- droplet
  Activated CCNs are called droplets. To better compare models using Twomey activation and models explicitly calculating the activation of CCNs, deliquescent aerosol particles and cloud/rain droplets are distinguished in this study. If CCN activation is explicitly considered, a particle is thought to be activated if the radius is larger than the critical radius $r_{\mathrm{crt}}=(3b/a)^{1/2}$ where a and b are parameters that represent the curvature effect and solution effect in the equilibrium supersaturation equation, $S_{\mathrm{eq}} \approx a/r - b/r^3$.
- cloudy grid cell
  A grid cell is considered cloudy if $(q_c+q_r) > 0.01\mathrm{g\ kg}^{-1}$
- n-th moment M_n
  $$M_n := \sum_i r_i^n.$$
- number of droplets N
  $$N = M_0.$$
- average of r^n
  $$\langle r^n \rangle := \sum_i r_i^n / N = M_n/M_0$$
- effective radius r_e
  $$r_{\mathrm{e}} := \langle r^3 \rangle / \langle r^2 \rangle = M_3/M_2$$
- standard deviation σ
  $$\sigma := \sqrt{\langle r^2 \rangle - \langle r \rangle^2} = \sqrt{M_2/M_0 - (M_1/M_0)^2}$$
- ratio of mean volume radius to effective radius cubed k
  $$k := \langle r^3 \rangle / {r_{\mathrm{e}}}^3 = \langle r^2 \rangle^3 / \langle r^3 \rangle^2 = M_2^3/M_0/M_3^2.$$
- adiabatic fraction AF
  AF at position $\boldsymbol{x}=(x,y,z)$ is defined by

$$\mathrm{AF}(\boldsymbol{x}) := \mathrm{LWC}(\boldsymbol{x})/\mathrm{ALWC}(\boldsymbol{x}).$$

Here, ALWC(***x***) is the adiabatic liquid water content, which can be evaluated as follows

$$\begin{aligned}\mathrm{ALWC}(\boldsymbol{x}) &= \rho(\boldsymbol{x}) q_{\mathrm{c}}^{\mathrm{ad}}(\boldsymbol{x}) \\ &= \rho(\boldsymbol{x})[q_{\mathrm{v}}^{\mathrm{sat}}(\text{cloud base}) - q_{\mathrm{v}}^{\mathrm{sat}}(\boldsymbol{x})] \\ &= \rho(\boldsymbol{x}) \frac{\rho_{\mathrm{v}}^{\mathrm{sat}}(T_{\mathrm{cb}})}{\rho_{\mathrm{cb}}} - \rho_{\mathrm{v}}^{\mathrm{sat}}\big(T(\boldsymbol{x})\big).\end{aligned}$$

Therefore, to use this formula, we have to estimate T_{cb} and ρ_{cb}, i.e., the temperature and density of the parcel when it was located at the cloud base. Cloud base height at a time *t* is the lowest cloudy grid at the time. Then, by horizontally averaging the profile around the cloud base, we can evaluate T_{cb} and ρ_{cb} at time *t*.

Example of Results

- 3D: https://drive.google.com/drive/folders/1AXDO6Ib8HGTfk1r7rEt4oVG4xkfAF7Lx
- 2D: https://drive.google.com/drive/folders/1pFs7xGKTfDEkl0l5gYYFbOv0_ZSb2RDa
- VR movie on youtube (created by Toshiki Matsushima): https://youtu.be/dxoIdczz-gc
  Best on VR headset. On your PC you can move it interactively by your mouse.

References

Brenguier, J.-L., Burnet, F., and Geoffroy, O.: Cloud optical thickness and liquid water path – does the k coefficient vary with droplet concentration?, Atmos. Chem. Phys., 11, 9771–9786, https://doi.org/10.5194/acp-11-9771-2011, 2011.

Grabowski, W. W., 2019: Separating physical impacts from natural variability using piggybacking (master-slave) technique. Adv. Geosci., 49, 105–111, 2019 https://doi.org/10.5194/adgeo-49-105-2019.

Grabowski, W. W., H. Morrison, S. Shima, G. C. Abade, P. Dziekan, and H. Pawlowska, 2018: Modeling of cloud microphysics: Can we do better? Bull. Amer. Meteor. Soc., 100, 655–672, https://doi.org/10.1175/BAMS-D-18-0005.1.

Lasher-Trapp, S.G., Cooper, W.A. and Blyth, A.M. (2005), Broadening of droplet size distributions from entrainment and mixing in a cumulus cloud. Q.J.R. Meteorol. Soc., 131: 195-220. https://doi.org/10.1256/qj.03.199.

Morrison, H., M. Witte, G. H. Bryan, J. Y. Harrington, and Z. J. Lebo, 2018: Broadening of modeled cloud droplet spectra using bin microphysics in an Eulerian spatial domain. J. Atmos. Sci., 75, 4005–4030, https://doi.org/10.1175/JAS-D-18-0055.1.